

Reduced-order models for flow control: balanced models and Koopman modes

Clarence W. Rowley, Igor Mezić, Shervin Bagheri, Philipp Schlatter, and Dan S. Henningson

Abstract This paper addresses recent developments in model-reduction techniques applicable to fluid flows. The main goal is to obtain low-order models tractable enough to be used for analysis and design of feedback laws for flow control, while retaining the essential physics. We first give a brief overview of several model reduction techniques, including Proper Orthogonal Decomposition [3], balanced truncation [8, 9], and the related Eigensystem Realization Algorithm [5, 6], and discuss strengths and weaknesses of each approach. We then describe a new method for analyzing nonlinear flows based on spectral analysis of the *Koopman operator*, a linear operator defined for any nonlinear dynamical system. We show that, for an example of a jet in crossflow, the resulting Koopman modes decouple the dynamics at different timescales more effectively than POD modes, and capture the relevant frequencies more accurately than linear stability analysis.

1 Introduction

The ability to effectively control a fluid would enable many exciting technological advances, including modifying the stability of laminar flows, and delaying transition from laminar to turbulent flow. Many of the tools available for analysis and design of control systems require knowledge of a model in terms of a system of differential equations, and the equations governing a fluid, though known, are too complex for these tools to apply. Model reduction addresses this problem: one obtains approx-

C.W. Rowley
Princeton University, USA, e-mail: cwrowley@princeton.edu

I. Mezić
University of California, Santa Barbara, USA e-mail: mezc@engineering.ucsb.edu

S. Bagheri, P. Schlatter, and D.S. Henningson
KTH, Stockholm, Sweden, e-mail: shervin.bagheri@mech.kth.se, pschlatt@mech.kth.se, hennings@mech.kth.se

imate models that are computationally tractable and capture the essential physics, but neglect details that are not critical for the problem at hand.

Here, we present a brief overview and comparison of various methods used for obtaining reduced-order models, aimed at applications in flow control. We then present a new method for analyzing fluid flows, based on spectral analysis of an object called the Koopman operator, and apply the method to a jet in crossflow.

2 Model reduction techniques

Many of the methods used for model reduction involve projecting known, high-dimensional dynamics onto a set of modes. For instance, for a state variable $q(t)$ (which could be a flow field at a specified time t), we begin with known dynamics $\dot{q}(t) = f(q)$ (for instance, the Navier-Stokes equations). Then we expand $q(t)$ in terms of a set of basis functions, or modes, φ_k :

$$q(t) = \sum_{k=1}^n a_k(t) \varphi_k. \quad (1)$$

If the modes φ_k are orthonormal, we obtain projected dynamics as $\dot{a}_k(t) = \langle f(q(t)), \varphi_k \rangle$. If the modes are not orthonormal (e.g., if they are eigenmodes of a non-normal operator A), then we often have a complementary set of *adjoint modes* ψ_j that satisfy $\langle \varphi_j, \psi_k \rangle = \delta_{jk}$ (e.g., eigenmodes of adjoint operator A^*). In this case, we still have the expansion (1), but the projected dynamics are given by $\dot{a}_k(t) = \langle f(q(t)), \psi_k \rangle$. In such projection methods, the main choices for obtaining reduced-order models are therefore how to choose the modes φ_j and ψ_k .

2.1 Proper Orthogonal Decomposition and its limitations

A common approach is to determine the modes φ_k by Proper Orthogonal Decomposition (POD) of a certain dataset [3]. While this approach is optimal for capturing the energy in a given dataset, this choice is often not appropriate for obtaining reduced-order models, since low-energy modes can be critically important for capturing the dynamics.

A striking example of the importance of low-energy modes is shown in [4], in which POD modes are computed from snapshots of the transient growth of a disturbance in a linearized channel flow. The first five POD modes capture over 99% of the energy, and yet the corresponding reduced-order model completely misses the transient energy growth. If, however, low-energy modes 10 and 17 are used in place of modes 4 and 5, the resulting five-mode model performs very well, and captures the transient growth nearly perfectly. While POD models can work well, this ex-

ample illustrates that they often require careful tuning, and one must be aware that low-energy modes can be critically important to the dynamics.

2.2 *Balanced models*

An alternative approach, popular in the control theory community, is balanced truncation [8]. This approach is applicable to linear systems, and has *a priori* error bounds that are close to the minimum possible error from any reduced-order model. In [9], an approximation of balanced truncation is introduced, called Balanced POD. In this method, the direct modes φ_j and adjoint modes ψ_k are computed from snapshots taken from a simulation of the original (linear) system and an adjoint system. Once these modes are known, the reduced-order models are computed as described above. This method, which approaches exact balanced truncation as the number of snapshots is increased, also corresponds to POD of a particular dataset (an impulse response) with respect to a particular inner product (called the observability Gramian). This inner product may be regarded as a measure of *dynamic* importance, and thus, the notion of “energy” in POD is simply redefined to refer to dynamic importance, rather than the usual (physical) energy.

In practice, this method often dramatically outperforms the standard POD method, particularly for highly non-normal systems. For instance, for the transient growth problem in [4] mentioned above, a 3-mode balanced model captures the transient growth nearly perfectly, and the models consistently improve as more modes are included, without any of the manual tweaking necessary for the POD models.

It is also worth noting that balanced models may also be obtained using the Eigensystem Realization Algorithm [5] (ERA). In fact, it has recently been shown that for linear systems, ERA produces reduced-order models that are identical to those from Balanced POD [6]. This method does not involve adjoint simulations, and hence can be used with experimental data. However, unlike Balanced POD, the Eigensystem Realization Algorithm does not produce modes φ_j, ψ_k , which can be useful for a variety of purposes, such as projection of nonlinear dynamics, or retaining parameters in the models. For more information about the advantages and disadvantages of ERA, see [6].

3 Spectral analysis of nonlinear flows

In this section, we describe a new method for analyzing the dynamics of nonlinear systems, based on spectral analysis of an object called the Koopman operator. The Koopman operator is a *linear* operator defined for any nonlinear system, but it is not based on linearization: indeed, it captures all of the dynamics of the full nonlinear system. The Koopman operator describes the evolution of *observables* on the phase space. For instance, an observable may be a 2D slice of velocity vectors obtained

from an experiment using Particle Image Velocimetry (PIV). Below, we define this operator, and the *Koopman modes* associated with a particular observable. For a more detailed explanation of this operator and its use, see [7, 10].

3.1 Koopman operator and Koopman modes

Consider a dynamical system evolving on a manifold M such that, for $\mathbf{x}_k \in M$,

$$\mathbf{x}_{k+1} = \mathbf{f}(\mathbf{x}_k), \quad (2)$$

where \mathbf{f} is a map from M to itself. The *Koopman operator* is a linear operator U that acts on scalar-valued functions on M in the following manner: for any scalar-valued function $g : M \rightarrow \mathbb{R}$, U maps g into a new function Ug given by

$$Ug(\mathbf{x}) = g(\mathbf{f}(\mathbf{x})). \quad (3)$$

Although the dynamical system is nonlinear and evolves on a finite-dimensional manifold M , the Koopman operator U is linear, but infinite-dimensional.

The idea is to analyze the flow dynamics governed by (2) only from available data—collected either numerically or experimentally—using the eigenfunctions and eigenvalues of U . To this end, let $\varphi_j : M \rightarrow \mathbb{R}$ denote eigenfunctions and $\lambda_j \in \mathbb{C}$ denote eigenvalues of the Koopman operator,

$$U\varphi_j(\mathbf{x}) = \lambda_j\varphi_j(\mathbf{x}), \quad j = 1, 2, \dots \quad (4)$$

and consider a vector-valued *observable* $\mathbf{g} : M \rightarrow \mathbb{R}^p$. For instance, if $\mathbf{x} \in M$ contains the full information about a flow field at a particular time, $\mathbf{g}(\mathbf{x})$ is a vector of any quantities of interest, such as a velocity measurements at various points in the flow. If each of the p components of \mathbf{g} lies within the span of the eigenfunctions φ_j , then as in [7], we may expand the vector-valued \mathbf{g} in terms of these eigenfunctions, as

$$\mathbf{g}(\mathbf{x}) = \sum_{j=1}^{\infty} \varphi_j(\mathbf{x}) \mathbf{v}_j. \quad (5)$$

We typically think of this expression as expanding the vector $\mathbf{g}(\mathbf{x})$ as a linear combination of the vectors \mathbf{v}_j , but we may alternatively think of this expression as expanding the function $\mathbf{g}(\cdot)$ as a linear combination of the eigenfunctions φ_j of U , where now \mathbf{v}_j are the (vector) coefficients in the expansion. In this paper, we will refer to the eigenfunctions φ_j as *Koopman eigenfunctions*, and the corresponding vectors \mathbf{v}_j in (5) the *Koopman modes* of the map \mathbf{f} , corresponding to the observable \mathbf{g} . Note that iterates of \mathbf{x}_0 are then given by

$$\mathbf{g}(\mathbf{x}_k) = \sum_{j=1}^{\infty} U^k \varphi_j(\mathbf{x}_0) \mathbf{v}_j = \sum_{j=1}^{\infty} \lambda_j^k \varphi_j(\mathbf{x}_0) \mathbf{v}_j. \quad (6)$$

The *Koopman eigenvalues*, $\lambda_j \in \mathbb{C}$, therefore characterize the temporal behavior of the corresponding Koopman mode \mathbf{v}_j : the phase of λ_j determines its frequency, and the magnitude determines the growth rate. Note that, as described in [7], for a system evolving on an attractor, the Koopman eigenvalues always lie on the unit circle.

3.2 Properties of Koopman modes and eigenvalues

It is not immediately clear why the Koopman modes and eigenvalues might be of interest in studying fluid flows. However, these modes are in fact related to objects routinely used in fluid mechanics, such as global eigenmodes (for linear systems) and the discrete Fourier transform (for periodic solutions of (2)). For a more detailed presentation, see [10], but here we summarize the main results:

- For a linear system ($\mathbf{x}_{k+1} = \mathbf{A}\mathbf{x}_k$), if the observable is the full state $\mathbf{g}(\mathbf{x}) = \mathbf{x}$, then the eigenvalues of \mathbf{A} are also Koopman eigenvalues, and the corresponding eigenvectors of \mathbf{A} are Koopman modes.
- For a nonlinear system with a periodic orbit, if we restrict the phase space to the periodic orbit, then the Koopman modes are given by the *discrete Fourier transform* of the vectors that make up the periodic orbit. In particular, if we have a set $S = \{\mathbf{x}_0, \dots, \mathbf{x}_{m-1}\}$ that forms a periodic solution of (2), such that $\mathbf{x}_{k+m} = \mathbf{x}_k$ for all k , then the discrete Fourier transform defines a new set of vectors $\{\hat{\mathbf{x}}_0, \dots, \hat{\mathbf{x}}_{m-1}\}$ that satisfy

$$\mathbf{x}_k = \sum_{j=0}^{m-1} e^{2\pi i j k / m} \hat{\mathbf{x}}_j, \quad k = 0, \dots, m-1. \quad (7)$$

Then the vectors $\hat{\mathbf{x}}_j$ are Koopman modes, with corresponding eigenvalues $\lambda_j = e^{2\pi i j / m}$. Thus, the phase $2\pi i j / m$ of the Koopman eigenvalue λ_j is the frequency of the corresponding mode $\hat{\mathbf{x}}_j$.

The Koopman modes therefore provide a framework that unifies linear stability theory (for transients of linear systems), and the discrete Fourier transform (for periodic solutions of nonlinear systems).

3.3 Computing Koopman modes from snapshots

The Koopman eigenvalues and modes would not be useful for practical applications if they could not be computed. It turns out that approximations to these modes and eigenvalues may be computed directly from snapshots of an observable, using a Krylov subspace method, a variant of the commonly used Arnoldi iteration [11]. The algorithm is in fact identical to that referred to as *Dynamic Mode Decomposition* in [12]. For the details of the algorithm, and its relation to Koopman modes, see [10].

3.4 Example: jet in crossflow

In this section we compute the Koopman modes for a jet in crossflow, and show that they directly allow an identification of various phenomena present in this flow. The parameters and the numerical code are the same as in the DNS performed in [2]; the jet inflow ratio is $R \equiv V_{\text{jet}}/U_\infty = 3$, the Reynolds number is $Re_{\delta_0^*} \equiv U_\infty \delta_0^*/\nu = 165$ and the ratio between the crossflow displacement thickness and the jet diameter is $\delta_0^*/D = 1/3$.

The empirical Ritz values λ_j and the empirical vectors \mathbf{v}_j are computed from a sequence of flow-fields $\{\mathbf{u}_0, \mathbf{u}_1, \dots, \mathbf{u}_{m-1}\} = \{\mathbf{u}(t = 200), \mathbf{u}(t = 202), \dots, \mathbf{u}(t = 700)\}$ with $m = 251$, using the algorithm mentioned in Section 3.3. The transient time ($t < 200$) is not sampled, and only the asymptotic motion in phase space is considered.

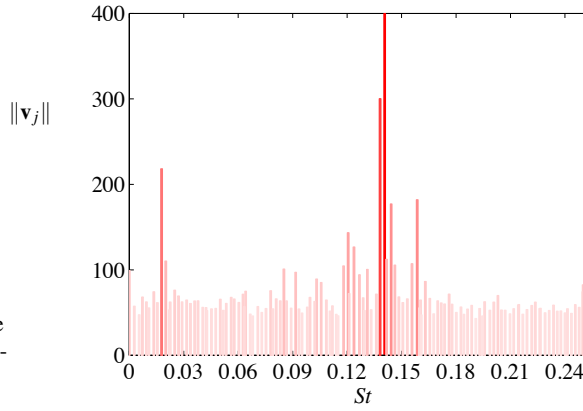


Fig. 1 The magnitudes of the Koopman modes \mathbf{v}_j , as a function of their nondimensional frequency $St = \omega D / (2\pi V_{\text{jet}})$.

The magnitudes of the modes, defined by the global energy norm $\|\mathbf{v}_j\|$, are shown in Figure 1, as a function of the corresponding frequency $\omega_j = \text{Im}\{\log(\lambda_j)\}/\Delta t$ (with $\Delta t = 2$ in our case). Only the $\omega_j \geq 0$ are shown, since the eigenvalues come in complex-conjugate pairs. Ordering the modes with respect to their magnitude, the first (2–3) and second (4–5) pair of modes oscillate with $St_2 = 0.141$ and $St_4 = 0.136$ respectively, whereas the third pair of modes (6–7) oscillate with $St_6 = 0.017$. All linear combinations of the frequencies excite higher modes: for instance, the nonlinear interaction of the first and third pair results in the fourth pair, i.e. $St_8 = 0.157$ and so on.

The frequencies of these dominant Koopman modes agree very well with frequencies obtained from point measurements of the DNS, taken from the shear layer and near-wall regions, respectively, as shown in Table 1.

The streamwise velocity component u of Koopman modes 2 and 6 are shown in Figure 2. Each mode represents a flow structure that oscillates with one single frequency, and the superposition of several of these modes results in the quasiperiodic

global system. The high-frequency mode 2 (Figure 2(a)) can be associated with shear layer vortices; along the jet trajectory there is first a formation of ring-like vortices that eventually dissolve into smaller scales due to viscous dissipation. Also visible are upright vortices: on the leeward side of the jet, there is a significant structure extending towards the wall. This indicates that the shear-layer vortices and the upright vortices are coupled and oscillate with the same frequency.

On the other hand, the low-frequency mode 6 shown in figure 2(b) features large-scale positive and negative streamwise velocity near the wall, which can be associated with shedding of the wall vortices. However, this mode also has structures along the jet trajectory further away from the wall. This indicates that the shedding of wall vortices is coupled to the jet body, *i.e.* the low frequency can be detected nearly anywhere in the vicinity of the jet since the whole jet is oscillating with that frequency.

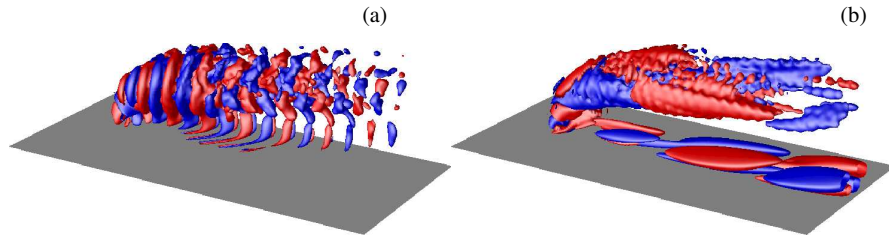


Fig. 2 Positive (red) and negative (blue) contour levels of the streamwise velocity components of two Koopman modes. The wall is shown in gray. (a) Mode 2, with $\|\mathbf{v}_2\| = 400$ and $St_2 = 0.141$. (b) Mode 6, with $\|\mathbf{v}_6\| = 218$ and $St_6 = 0.0175$.

3.5 Comparison with linear global modes and POD modes

The linear global eigenmodes of the Navier-Stokes equations linearized about an unstable steady state solution were computed by [2] for the same flow parameters as the current study. They computed 22 complex-conjugate unstable modes using the Arnoldi method combined with a time-stepper approach. The frequency of the most unstable (anti-symmetric) mode associated with the shear-layer instability was $St = 0.169$, not far from the value $St = 0.14$ observed for the DNS. However, the mode with the lowest frequency associated with the wall vortices was $St = 0.043$, far from the observed frequency of $St = 0.017$. These frequencies are summarized in Table 1. The global eigenmodes capture the dynamics only in a neighborhood of the unstable fixed point, while the Koopman modes correctly capture the behavior on the attractor.

We also compared the Koopman modes with modes determined by Proper Orthogonal Decomposition (POD) of the same dataset. The POD modes themselves are shown in [1], and capture similar spatial structures to the Koopman modes shown in Figure 2. The most striking distinction is in the time coefficients: while a single

Mode	DNS	Global	POD	Koopman
Shear layer	0.141	0.169	0.138, 0.158, 0.121	0.141
Wall	0.017	0.043	0.0188, 0.0094, 0.158, 0.121	0.017

Table 1 Comparison of the frequencies ($St = fD/V_{\text{jet}}$) obtained from DNS probes; the global eigenmodes of the linearized Navier-Stokes; POD modes 1 and 6, corresponding to mainly shear-layer and wall oscillations, respectively; and Koopman modes.

Koopman mode contains, by construction, only a single frequency component, the POD modes capture the most energetic structures, resulting in modes that contains several frequencies. For situations such as the jet in crossflow where one is interested in studying the dynamics of low-frequency oscillations (such as wall modes) separate from high-frequency oscillations (such as shear-layer modes), the Koopman modes are thus more effective at decoupling and isolating these dynamics.

Acknowledgments

This work was supported by the National Science Foundation, award CMS-0347239, and the Air Force Office of Scientific Research, awards FA9550-05-1-0369 and FA9550-07-1-0127.

References

1. S. Bagheri, P. Schlatter, and D. S. Henningson. Self-sustained global oscillations in a jet in crossflow. *Theor. Comput. Fluid Dyn.*, (submitted), 2009.
2. S. Bagheri, P. Schlatter, P. Schmid, and D. S. Henningson. Global stability of a jet in crossflow. *J. Fluid Mech.*, 624:33–44, 2009.
3. P. Holmes, J. L. Lumley, and G. Berkooz. *Turbulence, Coherent Structures, Dynamical Systems and Symmetry*. Cambridge University Press, Cambridge, UK, 1996.
4. M. Ilak and C. W. Rowley. Modeling of transitional channel flow using balanced proper orthogonal decomposition. *Phys. Fluids*, 20:034103, March 2008.
5. J.-N. Juang and S. Pappa, Richard. An eigensystem realization algorithm for modal parameter identification and model reduction. *J. Guid. Contr. Dyn.*, 8(5):620–627, 1985.
6. Z. Ma, S. Ahuja, and C. W. Rowley. Reduced order models for control of fluids using the eigensystem realization algorithm. *Theor. Comput. Fluid Dyn.*, (submitted), 2009.
7. I. Mezić. Spectral properties of dynamical systems, model reduction and decompositions. *Nonlin. Dyn.*, 41:309–325, 2005.
8. B. C. Moore. Principal component analysis in linear systems: Controllability, observability, and model reduction. *IEEE Trans. Automat. Contr.*, 26(1):17–32, Feb. 1981.
9. C. W. Rowley. Model reduction for fluids using balanced proper orthogonal decomposition. *Int. J. Bifurcation Chaos*, 15(3):997–1013, Mar. 2005.
10. C. W. Rowley, I. Mezić, S. Bagheri, P. Schlatter, and D. S. Henningson. Spectral analysis of nonlinear flows. *J. Fluid Mech.*, (submitted), 2009.
11. A. Ruhe. Rational Krylov sequence methods for eigenvalue computation. *Linear Algebra Appl.*, 58:391–405, 1984.
12. P. Schmid and J. Sesterhenn. Dynamic mode decomposition of numerical and experimental data. 61st Annual Meeting of the APS Division of Fluid Dynamics, Nov. 2008.